Intradot time scales strongly affect the relaxation dynamics in quantum dot lasers

M. Abusaa,[1,2] J. Danckaert,[1] E. A. Viktorov,[1,3] and T. Erneux[3]
[1]*Applied Physics Research Group (APHY), Vrije Universiteit Brussel, Pleinlaan 2, B-1050 Brussels, Belgium*
[2]*Physics Department, Arab American University, Al Zababeda, Jenin, Palestine*
[3]*Optique Nonlinéaire Thréorique, Université Libre de Bruxelles, Campus Plaine Code Postale 231, B-1050 Bruxelles, Belgium*
(Received 24 January 2013; published 17 June 2013)

We analyze an electron-hole asymmetry model for simultaneous two-state operation in semiconductor quantum dot lasers. From the linearized equations, we determine simple analytical expressions for the relaxation oscillation (RO) frequencies. Of particular interest is the fact that different expressions for the RO frequencies are obtained depending on the relative values of the photon lifetime and the basic time scale of the nonlinear intradot interaction. If comparable, we find only one frequency that depends on a combination of the two-state intensities.

DOI: 10.1103/PhysRevA.87.063827 PACS number(s): 42.60.Rn, 42.55.Px, 78.67.Hc

I. INTRODUCTION

Semiconductor quantum dot (QD) lasers are extensively studied for applications in future telecommunications systems. Compared to the advantages of the quantum well laser that preceded it, improvements in modulation bandwidth, lasing threshold, relative intensity noise, and temperature insensitivity have all been observed [1]. The discrete structure of the energy levels in QD allows simultaneous lasing at the ground (GS) and excited (ES) states [2]. At low currents, the recombination of a GS electron-hole pair results in GS emission. Increasing the injection current leads to a larger population of the ES, to the appearance of a second threshold, and to dual (simultaneous) lasing in both the GS and the ES. The simultaneous lasing has been already investigated in steady-state operations [3,4], in specific dynamical regimes [5–7], and mode locking [8,9]. But analytical investigations such as determining a physically relevant expression for the relaxation oscillation (RO) frequency is still missing. In this paper, we propose such an analysis starting from a full rate equation model that takes care of both the emissions from the GS and ES.

Damped ROs is a key observation for all semiconductor lasers as well as for other class *B* lasers that include solid state and CO_2 lasers [10]. The weak damping of the ROs compared to the time scale of the oscillations also explains why the laser is highly sensitive to external perturbations. In particular, a periodic modulation at a frequency close to the RO frequency leads to a significant resonant response that is used for many applications in optical communications, data storage, environmental monitoring, etc. More resonant frequencies appear in the multimode regime of operation and result from the mode-to-mode coupling. These frequencies are known as antiphase RO frequencies as the perturbed lasing modes slowly oscillate back to the steady state with phase-shifted oscillations [11].

The ROs in a single-mode QD laser operating at the GS were analytically examined in detail [12,13]. In this paper, we analyze an electron-hole asymmetry model for two-state lasing which has been first suggested in Ref. [3] and determine an approximation of the RO based on the natural values of the laser parameters. We find that the capture and escape processes between the GS and ES may have a pronounced effect on the ROs. Specifically, we find a significant increase of the RO frequency with the appearance of simultaneous lasing at both GS and ES, as has been previously observed experimentally [14]. This effect can be important for multiple technological applications with a high speed modulated optical signal.

The objective of this paper is twofold. We first substantiate the experimental results in Ref. [14] by finding that the RO frequency in the two-state lasing regime is not a function of the total intensity, as we naively could expect. Second, we emphasize the role of an additional material time scale provided by the intradot interactions. This time scale needs to be compared to the carrier lifetimes in order to properly derive the RO frequency.

The plan of the paper is as follows. The model rate equations are introduced in Sec. II. The steady-state solutions are determined analytically in Sec. III and a relevant approximation for the intensities is derived. In Sec. IV, we investigate the linearized equations and determine two distinct approximations of the RO frequency. Our approximations are compared to the numerical solutions obtained from the linearized equations. The validity of our analysis and future plans are discussed in Sec. V.

II. RATE EQUATIONS

The electron-hole asymmetry model consists of rate equations for the electromagnetic field intensities ($I_{g,\mathrm{ex}}$) and GS and ES occupational probabilities for electrons and holes ($n^g_{e,h}$,$n^{\mathrm{ex}}_{e,h}$), and the carriers in a wetting layer ($w_{e,h}$). The model equations are an extension of the equations formulated in Ref. [3] that includes contributions from the wetting layer. In dimensionless form, they are given by

$$\dot{I}_g = \left[2g\left(n^g_e + n^g_h - 1\right) - 1\right] I_g, \tag{1}$$

$$\dot{I}_{\mathrm{ex}} = \left[4g\left(n^{\mathrm{ex}}_e + n^{\mathrm{ex}}_h - 1\right) - 1\right] I_{\mathrm{ex}}, \tag{2}$$

$$\dot{n}^g_{e,h} = \eta\left[2F_{e,h} - n^g_e n^g_h - g\left(n^g_e + n^g_h - 1\right) I_g\right], \tag{3}$$

$$\dot{n}^{\mathrm{ex}}_{e,h} = \eta\big[B^w_{e,h} w_{e,h}\left(1 - n^{\mathrm{ex}}_{e,h}\right) - R_{e,h} n^{\mathrm{ex}}_{e,h} - F_{e,h} - n^{\mathrm{ex}}_e n^{\mathrm{ex}}_h - g\left(n^{\mathrm{ex}}_e + n^{\mathrm{ex}}_h - 1\right) I\big], \tag{4}$$

$$\dot{w}_{e,h} = \eta\big[J - w_e w_h - 4B^w_{e,h} w_{e,h}\left(1 - n^{\mathrm{ex}}_{e,h}\right) + 4R_{e,h} n^{\mathrm{ex}}_{e,h}\big], \tag{5}$$

where the dot means differentiation with respect to $t \equiv t'/\tau_{\rm ph}$. t' is the original time and $\tau_{\rm ph}$ is the photon lifetime. $\eta \equiv \tau_{\rm ph}\tau^{-1} \ll 1$, where τ denotes the carrier recombination time. The factors 2 and 4 account for the degeneracy in the QD energy levels. J is the pump current per dot. The gains $2g(n_e^g + n_h^g - 1)$ and $4g(n_e^{\rm ex} + n_h^{\rm ex} - 1)$ are defined by the dot population and a g factor. We define g as the effective gain factor scaled to the cavity losses, and assume the gain factors and the cavity losses to be identical for both GS and ES. The nonlinear interaction $F_{e,h} \equiv B_{e,h}n_{e,h}^{\rm ex}(1 - n_{e,h}^g) - C_{e,h}n_{e,h}^g(1 - n_{e,h}^{\rm ex})$ between the different states is provided by the Pauli blocking factor $(1 - n_{e,h}^{g,{\rm ex}})$. $B_{e,h}(C_{e,h})$ and $B_{e,h}^w(R_{e,h})$ are defined as the capture (escape) rates to (from) the GS and the ES, respectively. The charge neutrality remains fully preserved in the model.

The model (1)–(5) supports the GS intensity decrease during the simultaneous lasing regime for a specific range of values of the parameters but is too complicated for analytical investigations. We consider a number of simplifications which qualitatively preserve the dynamical properties of the full rate equations model and which allow us to determine analytical expressions of physical significance. Specifically, we assume a direct pumping of the ES from the wetting layer represented by the rates J, and replace $B_{e,h}^w w_{e,h}(1 - n_{e,h}^{\rm ex})$ with $J(1 - n_{e,h}^{\rm ex})$ in Eq. (4). The slowness of the recombination processes motivates neglecting the terms $n_e^{g,{\rm ex}}n_h^{g,{\rm ex}}$. We assume that electrons and holes are captured with the same rates $B_e = B_h = B$. To determine the escape rates $C_{e,h}$, we use the Kramers relation [15] linking the capture $B_{e,h}$ and the escape $C_{e,h}$ rates,

$$C_{e,h} = B_{e,h}\exp(-\Delta E_{e,h}/\kappa_B T), \tag{6}$$

where κ_B is the Boltzmann constant and T is the plasma temperature. We assume that the electron mass is ten times the hole mass, and estimate the hole and electron energy level spacing as $\Delta E_h \approx 5$ meV and $\Delta E_e \approx 50$ meV. At room temperature, $\kappa_B T = 25$ meV, so that $\Delta E_h \ll \kappa_B T$ and $\Delta E_e \gg \kappa_B T$. It leads to the approximation $C_e = 0$ and $C_h = B$, and the electron-hole redistribution rate asymmetry [3]. Typical values of the recombination time (1 ns), GS capture time (10 ps), and the photon lifetime (10 ps) imply $\eta = 0.01$ and $B = 100$.

These assumptions then lead to the following reduced model:

$$\dot I_g = \left[2g\left(n_e^g + n_h^g - 1\right) - 1\right] I_g, \tag{7}$$

$$\dot I_{\rm ex} = \left[4g\left(n_e^{\rm ex} + n_h^{\rm ex} - 1\right) - 1\right] I_{\rm ex}, \tag{8}$$

$$\dot n_e^g = \eta\left[2Bn_e^{\rm ex}\left(1 - n_e^g\right) - \left(n_e^g + n_h^g - 1\right) I_g\right], \tag{9}$$

$$\dot n_e^{\rm ex} = \eta\big[J\left(1 - n_e^{\rm ex}\right) - R_e n_e^{\rm ex} - Bn_e^{\rm ex}\left(1 - n_e^g\right) - \left(n_e^{\rm ex} + n_h^{\rm ex} - 1\right) I_{\rm ex}\big], \tag{10}$$

$$\dot n_h^g = \eta\left[2B\left(n_h^{\rm ex} - n_h^g\right) - \left(n_e^g + n_h^g - 1\right) I_g\right], \tag{11}$$

$$\dot n_h^{\rm ex} = \eta\big[J\left(1 - n_h^{\rm ex}\right) - R_h n_h^{\rm ex} - B\left(n_h^{\rm ex} - n_h^g\right) - \left(n_e^{\rm ex} + n_h^{\rm ex} - 1\right) I_{\rm ex}\big]. \tag{12}$$

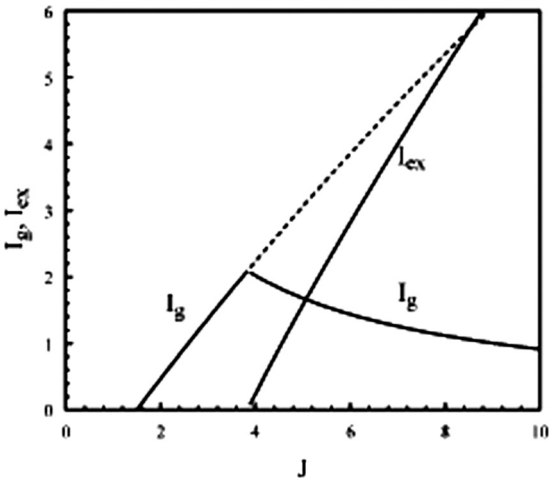

FIG. 1. Bifurcation diagram of steady states. A single GS lasing state emerges at the laser threshold $J_{\rm th} \approx 1.8$ and undergoes a secondary bifurcation to a two-lasing state at $J_{\rm gs} \approx 4$. Solid and dashed lines denote stable and unstable solutions. The values of the parameters are $g = 0.75$, $B = 100$, $R_h = 0.75$, and $R_e = 1$.

The model (7)–(12) fully preserves the intradot interactions limited by the Pauli blocking factor. Understanding the impact of these interactions on the dynamical properties of a QD laser is precisely the objective of our work. Mathematically, our dynamical problem depends on two small parameters, namely, η and B^{-1}. Physically, these two parameters are the normalized photon lifetime $\tau_{\rm ph}\tau^{-1}$ and the normalized capture time $\tau_c\tau^{-1}$. The parameter $\eta \approx 10^{-3} - 10^{-2}$ describes the slow relaxation of the carriers with respect to the photon lifetime, which is a common feature for all semiconductor lasers. The value of η affects the modulational bandwidth of these devices. The parameter $B^{-1} \approx 10^{-2}$ measures the effectiveness of the nonlinear intradot interaction. As we shall demonstrate, different scalings between η and B^{-1} may lead to significantly different RO frequencies.

III. STEADY STATES

In addition to the zero intensity solution, there exist three nonzero intensity steady states, namely, (i) $I_g \neq 0$, $I_{\rm ex} = 0$, (ii) $I_g \neq 0$, $I_{\rm ex} \neq 0$, and (iii) $I_g = 0$, $I_{\rm ex} \neq 0$. We are interested in the transition from (i) to (ii) and the bifurcation properties of the two-state regime (ii). The steady-state solutions can be determined analytically and admit simple expressions in the large B limit (fast capture rates). Fast capture rates are observed for most QD lasers, and this limit will be used when we determine approximations of the RO frequency in Sec. IV.

The single-mode GS regime (i) is stable up to a second threshold where the ES lasing regime emerges. The GS intensity increases with the injection current, as shown in Fig. 1. It satisfies the following quadratic equation:

$$-\frac{I_g}{2B}\left(2J - \frac{1}{4g}I_g + R_e\right) + \left(2g\frac{J - \frac{1}{4g}I_g}{J + R_h} - 1\right)\left(J - \frac{1}{4g}I_g\right) = 0. \tag{13}$$

Inserting $I_g = 0$ into Eq. (13) leads to the first laser threshold given by

$$J = J_{\rm th} \equiv \frac{R_h}{2g-1}. \tag{14}$$

In the large B limit, a simple expression for I_g can be determined from Eq. (13). We find

$$I_g \approx 2\,(2g-1)\,(J - J_{\rm th}) \geqslant 0. \tag{15}$$

Equation (15) indicates that the intensity is an $O(1)$ quantity independent of B. Using Eq. (15), we determine approximations for $n^g_{e,h}$ and $n^{\rm ex}_{e,h}$ from their exact expressions. They are given by

$$n^{\rm ex}_e = \frac{J + R_h}{2g\,(J + R_e)}, \tag{16}$$

$$n^{\rm ex}_h = n^g_h = \frac{1}{2g}, \tag{17}$$

$$n^g_e = 1 - \frac{1}{4gBn^{\rm ex}_e} I_g. \tag{18}$$

We note that $n^{\rm ex}_e$ depends on J, but quickly saturates at the $n^{\rm ex}_e = 1/(2g)$ as J increases. $n^{\rm ex}_h$ and n^g_h are both independent of J, in the first approximation. n^g_e is close to 1, but the $O(B^{-1})$ correction term in (18) is important for the correct estimation of the RO frequency in Sec. IV.

The two-state lasing regime (ii) strongly depends on all the material parameters, namely, the gain factor g, and the capture and escape rates B and $R_{e,h}$. The two intensities are given by

$$I_g = B\frac{4g-3-2\varepsilon_1}{(2+\varepsilon_1)}\frac{1}{\left(\frac{4g(2+\varepsilon_2)}{1+4g}+1\right)} > 0, \tag{19}$$

$$I_{\rm ex} = 4gJ - \frac{1+4g}{(2+\varepsilon_2)}(J+R_e) - I_g \geqslant 0, \tag{20}$$

where $\varepsilon_1 \equiv \frac{R_h - R_e}{J+R_e}$ and $\varepsilon_2 \equiv \frac{R_e - R_h}{J+R_h}$. The second threshold $J = J_{ge}$ is defined as the critical point where the two-state regime appears as we progressively increase J from $J_{\rm th}$. It satisfies the conditions $I_{\rm ex} = 0$ and $I_g > 0$, which can be solved analytically. Figure 2 shows J_{ge} as a function of g for two different values of B. All curves emerge from a critical point $(g, J) = (g_c, J_c)$ (dot in the figure) where the GS and GS-ES thresholds coalesce. g_c is given by

$$g_c = \frac{3R_e + \sqrt{9R_e^2 + 8R_e\,(R_h - R_e)}}{8R_e}, \tag{21}$$

and $J_c = J_{\rm th}(g_c)$ is given by (14). J_{ge} increases almost linearly with g and the slope increases with B. While both $\varepsilon_{1,2}$ are vanishing with J, I_g is proportional to $4g - 3 - 2\varepsilon_1$, which is the main factor controlling the inequality in Eq. (19). It underlines the effect of g and the difference $|R_e - R_h|$ which appears in ε_1.

If $g = 3/4$, I_g and $I_{\rm ex}$, given by (19) and (20), become

$$I_g = \frac{1}{\left(\frac{3(2+\varepsilon_2)}{4}+1\right)}\frac{-2\varepsilon_1 B}{(2+\varepsilon_1)} > 0, \tag{22}$$

$$I_{\rm ex} = 3J - 4(J+R_e)()\left(\frac{1}{2+\varepsilon_2}\right) - I_g \geqslant 0, \tag{23}$$

which requires the condition $\varepsilon_1 < 0$. Moreover, we note from (22) that I_g is an $O(1)$ quantity if $|\varepsilon_1|$ is $O(B^{-1})$ small. This

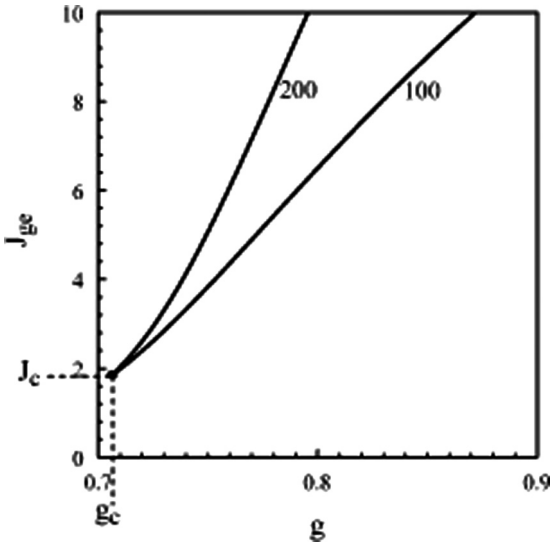

FIG. 2. Second threshold. The critical pump rate J_{ge} is shown as a function of g for $B = 100$ and $B = 200$ (lines are labeled by the value of B). The two curves emerge from a critical point where $I_{\rm ex} = I_g = 0$ (dot in the figure). The values of the fixed parameters are $R_h = 0.75$ and $R_e = 1$.

implies that $|R_h - R_e| = O(B^{-1})$. In this case, Eqs. (22) and (23) reduce to the expressions

$$I_g \approx \frac{2}{5}B\frac{R_e - R_h}{(J+R_e)}, \tag{24}$$

$$I_{\rm ex} \approx J - 2R_e - I_g > 0. \tag{25}$$

In the large B limit, Eqs. (24) and (25) show that the GS output intensity I_g decreases with J and vanishes in the limit of large pumping currents. On the other hand, the ES output $I_{\rm ex}$ steadily increases.

If $g \neq 3/4$, we find from (19) and (20) that both I_g and $I_{\rm ex}$ are $O(B)$ large quantities in the large B limit, regardless of the values of ε_1 and ε_2. Because of the inequality in (20), we also need to assume $J = O(B)$. If $|R_h - R_e| = O(B^{-1})$, we may neglect ε_1 and ε_2 in (19) and (20) and formulate simpler expression for the two intensities. They are given by

$$I_g = B\left(\frac{1+4g}{1+12g}\right)\left(\frac{4g-3}{2}\right) > 0, \tag{26}$$

$$I_{\rm ex} = \frac{4g-1}{2}J - \frac{4g+1}{2}R_e - I_g \geqslant 0. \tag{27}$$

The fact that $J = O(B)$ implies that the second threshold $J = J_{ge}$ increases to higher values as g progressively deviates from $g = 3/4$ ($g > 3/4$). Moreover, I_g will progressively become flatter. Figure 3 illustrates this evolution by showing the diagram of the stable steady states for two different values of g. This tendency is similar to the excitonic models of the two-state lasing [2]. We find that larger values of the g factor prevent the decrease of the GS output. It may explain that the experimentally observed decrease of the GS for operation at 1.3 μm [2,3] is not reported for an operating wavelength of 1.5 μm [16]. The QD materials operating at 1.5 μm reportedly possess a stronger gain ($\approx$30 cm^{-1}) compared to the gain

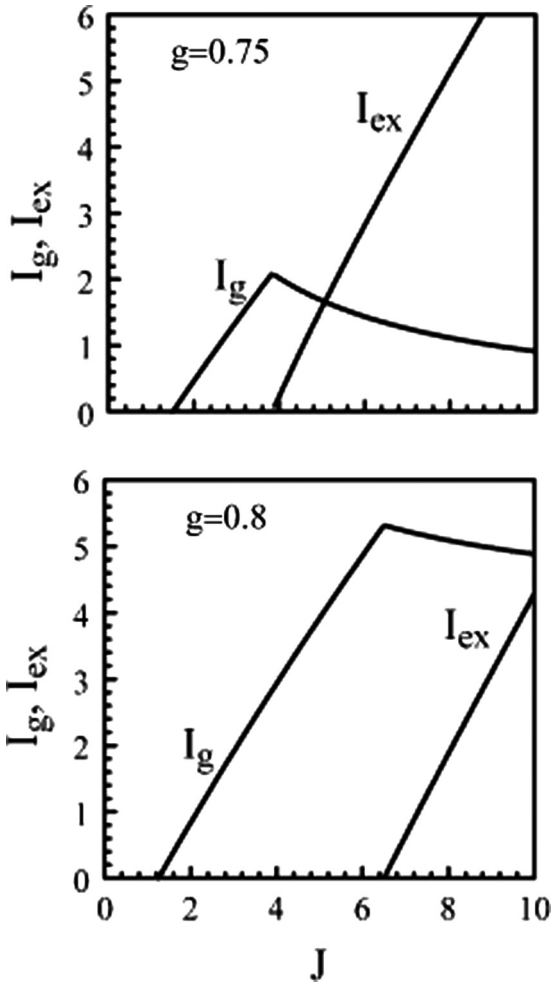

FIG. 3. Bifurcation diagrams of the stable steady states. $B = 100$, $R_h = 0.75$, and $R_e = 1$. If $g = 0.75$, the secondary bifurcation appears at $J \approx 4$ and I_g decreases with J. If $g > 0.75$, the secondary bifurcation point moves to higher amplitudes and I_g approaches a constant.

($\approx$15 cm^{-1}) of the QD materials with the wavelength centered at 1.3 μm.

IV. RELAXATION OSCILLATIONS

The two RO frequencies of a two-mode class B laser are known to exhibit some general properties [10,17]. Specifically, the largest frequency is determined by the total intensity and the second frequency characterizes the energy exchange between the two modes. Antiphase dynamics in lasers resulting from the energy exchange has been observed in numerous devices. The minimal requirements to observe antiphase effects were derived in Ref. [18] and suggest a strong spectral and spatial overlapping between the lasing modes. The GS and ES lasing transitions, in the QD problem, differ by $\Delta = 55$ meV and the overlapping of the modes is negligible. It is confirmed by experimentally observed weak antiphase fluctuations at a low sub-MHz frequency [5]. The frequency range of these antiphase fluctuations compared to the GHz frequency range of RO suggests an extremely weak cross coupling, which can be addressed to inhomogeneous broadening. For these reasons, the dynamical properties of our two-state QD laser are quite different from the one observed for a conventional two-mode laser.

Our analysis distinguishes two cases. We first consider the limit $\eta \to 0$ (B fixed) which applies for all class B lasers [11]. For the single GS lasing ($I_g \neq 0$ and $I_{ex} = 0$), the linear stability analysis leads to an expression for the RO frequency which is similar to the excitonic model [13],

$$\omega = \sqrt{2 I_g \eta}. \tag{28}$$

Solving numerically the full characteristic equation, we find a pair of complex eigenvalues with an imaginary part close to the approximation (28) but only for very low values of η ($\eta = 10^{-4}$ and $B = 10^2$). If $\eta = 10^{-2}$ and $B = 10^2$, we numerically find a different frequency. For the two lasing states ($I_g \neq 0$ and $I_{ex} \neq 0$), the limit $\eta \to 0$ (B fixed) leads to two separated equations describing harmonic oscillations with the frequencies

$$\omega_{g,\mathrm{ex}} = \sqrt{2 I_{g,\mathrm{ex}} \eta}. \tag{29}$$

Despite the fact that the two RO frequencies can be sufficiently different, neither of the two frequencies can be associated with an energy exchange between modes, as we observe for conventional multimode lasers. Again, we numerically find these frequencies only if η is sufficiently small compared to B.

The approximations of (27) and (28) are correct if ηB is sufficiently small but are not appropriate for the more realistic experimental range where $\eta B = O(1)$. To properly analyze this case, we need to relate the two small parameters η and B^{-1}. Specifically, we propose to scale η as $\eta = B^{-1}\eta_1$ where $\eta_1 = O(1)$ and explore the limit B large of the linearized equations. These scalings suggest that the photon lifetime τ_{ph} is similar to the capture time τ_{cap}, which is verified for most QD lasers.

We introduce $y_{g,\mathrm{ex}}$ and $x_{e,h}^{g,\mathrm{ex}}$ as the small deviations of $I_{g,\mathrm{ex}}$ and $n_{e,h}^{g,\mathrm{ex}}$ from their steady-state values, respectively. Equations (7)–(12) depend on many parameters and we limit our linear stability analysis to the case $g = 3/4$ and $\varepsilon_1 = O(B^{-1})$. The steady-state intensities I_g and I_{ex} are then given by Eqs. (24) and (25) in the large B limit. The linearized equations are given by

$$\dot{y}_g = 2g\left(x_e^g + x_h^g\right) I_g, \tag{30}$$

$$\dot{y}_{\mathrm{ex}} = 4g\left(x_e^{\mathrm{ex}} + x_h^{\mathrm{ex}}\right) I_{\mathrm{ex}}, \tag{31}$$

$$\dot{x}_e^g = \eta\big[2Bx_e^{\mathrm{ex}}\left(1 - n_e^g\right) - 2Bn_e^{\mathrm{ex}}x_e^g - \left(n_e^g + n_h^g - 1\right) y_g - \left(x_e^g + x_h^g\right) I_g\big], \tag{32}$$

$$\dot{x}_e^{\mathrm{ex}} = \eta\big[-Jx_e^{\mathrm{ex}} - R_e x_e^{\mathrm{ex}} - Bx_e^{\mathrm{ex}}\left(1 - n_e^g\right) + Bn_e^{\mathrm{ex}}x_e^g - \left(n_e^{\mathrm{ex}} + n_h^{\mathrm{ex}} - 1\right) y_{\mathrm{ex}} - \left(x_e^{\mathrm{ex}} + x_h^{\mathrm{ex}}\right) I_{\mathrm{ex}}\big], \tag{33}$$

$$\dot{x}_h^g = \eta\big[2B\left(x_h^{\mathrm{ex}} - x_h^g\right) - \left(n_e^g + n_h^g - 1\right) y_g - \left(x_e^g + x_h^g\right) I_g\big], \tag{34}$$

$$\dot{x}_h^{\mathrm{ex}} = \eta\big[-Jx_h^{\mathrm{ex}} - R_h x_h^{\mathrm{ex}} - B\left(x_h^{\mathrm{ex}} - x_h^g\right) - \left(n_e^{\mathrm{ex}} + n_h^{\mathrm{ex}} - 1\right) y_{\mathrm{ex}} - \left(x_{\mathrm{ex}}^{\mathrm{ex}} + x_h^{\mathrm{ex}}\right) I_{\mathrm{ex}}\big], \tag{35}$$

where I_g,$n_e^{\rm ex}$ . . . now denote their steady-state values. In these equations, we note that B multiplies (i) $x_e^{\rm ex}(1-n_e^g)$, (ii) x_e^g, (iii) $(x_h^{\rm ex}-x_h^g)$, and (iv) x_h^g. The first term is proportional to B^{-1} because of (18) and is $O(1)$ if multiplied by the coefficient B. The three other terms, however, need to be proportional to B^{-1} in order to counterbalance the effect of the large B coefficient. To this end, we introduce the following variables:

$$x_e^g = B^{-1}z_e^g, \tag{36}$$

$$x_h^{\rm ex} = u + B^{-1}z_h^{\rm ex}, \tag{37}$$

$$x_h^g = u + B^{-1}z_h^g. \tag{38}$$

Inserting Eqs. (36)–(38) into Eqs. (30)–(35) leads to the following problem:

$$\dot{y}_g = 2g\left(B^{-1}z_e^g + u + B^{-1}z_h^g\right)I_g, \tag{39}$$

$$\dot{y}_{\rm ex} = 4g\left(x_e^{\rm ex} + u + B^{-1}z_h^{\rm ex}\right)I_{\rm ex}, \tag{40}$$

$$B^{-1}\dot{z}_e^g = \eta\left[x_e^{\rm ex}\frac{I_g}{2gn_e^{\rm ex}} - 2n_e^{\rm ex}z_e^g - \frac{y_g}{2g} - \left(B^{-1}z_e^g + u + B^{-1}z_h^g\right)I_g\right], \tag{41}$$

$$\dot{x}_e^{\rm ex} = \eta\left[-Jx_e^{\rm ex} - R_e x_e^{\rm ex} - x_e^{\rm ex}\frac{I_g}{4gn_e^{\rm ex}} + n_e^{\rm ex}z_e^g - \frac{y_{\rm ex}}{4g} - \left(x_e^{\rm ex} + u + B^{-1}z_h^{\rm ex}\right)I_{\rm ex}\right], \tag{42}$$

$$\dot{u} + B^{-1}\dot{z}_h^g = \eta\left[2\left(z_h^{\rm ex} - z_h^g\right) - \frac{y_g}{2g} - \left(B^{-1}z_e^g + u + B^{-1}z_h^g\right)I_g\right], \tag{43}$$

$$\dot{u} + B^{-1}\dot{z}_h^{\rm ex} = \eta\left[-(J+R_h)\left(u + B^{-1}z_h^{\rm ex}\right) - \left(z_h^{\rm ex} - z_h^g\right) - \frac{y_{\rm ex}}{4g} - \left(x_e^{\rm ex} + u + B^{-1}z_h^{\rm ex}\right)I_{\rm ex}\right]. \tag{44}$$

Using (43) and (44), we determine an equation for $z_h^{\rm ex} - z_h^g$. We obtain

$$B^{-1}\left(\dot{z}_h^{\rm ex} - \dot{z}_h^g\right) = \eta\left[-(J+R_h)u - 3\left(z_h^{\rm ex} - z_h^g\right) + \frac{1}{2g}y_g + uI_g - \frac{1}{4g}y_{\rm ex} - \left(x_e^{\rm ex} + u\right)I_{\rm ex} + O(B^{-1})\right]. \tag{45}$$

Provided $B\eta$ is sufficiently large, we may eliminate x_e^g and $z_h^{\rm ex} - z_h^g$ from Eqs. (40) and (44), respectively. The linearized problem then reduces to four equations for the variables y_g, $y_{\rm ex}$, $x_e^{\rm ex}$, and u. Neglecting all B^{-1} small terms and formulating an equation for $v \equiv y_g + y_{\rm ex}$, we note that our four variable equations can be reduced to the following three variable equations for v, $x_e^{\rm ex}$, and u:

$$\dot{v} = (2gI_g + 4gI_{\rm ex})u + 4gI_{\rm ex}x_e^{\rm ex}, \tag{46}$$

$$\dot{x}_e^{\rm ex} = \eta\left[-(J + R_e + I_{\rm ex})x_e^{\rm ex} - \frac{v}{4g} - u\left(I_{\rm ex} + \frac{I_g}{2}\right)\right], \tag{47}$$

$$\dot{u} = \eta\left[-\frac{2}{3}\left(J + R_h + I_{\rm ex} + \frac{1}{2}I_g\right)u - \frac{v}{6g} - \frac{2}{3}x_e^{\rm ex}I_{\rm ex}\right]. \tag{48}$$

From the Jacobian of the last three equations, we determine the characteristic equation for the growth rate λ. It is given by

$$\lambda^3 - T_1\lambda^2 + T_2\lambda - T_3 = 0, \tag{49}$$

where

$$T_1 = -(J + R_e + I_{\rm ex})\eta - \frac{2}{3}\left(J + R_h + I_{\rm ex} + \frac{1}{2}I_g\right)\eta, \tag{50}$$

$$T_2 = \frac{\eta}{3}(I_g + 5I_{\rm ex}) + \eta^2\frac{2}{3}\left[(J+R_e)\left(J + R_h + I_{\rm ex} + \frac{1}{2}I_g\right) + I_{\rm ex}(J + R_h)\right], \tag{51}$$

$$T_3 = -\frac{\eta^2}{3}[2I_{\rm ex}(J + R_h) + (I_g + 2I_{\rm ex})(J + R_e)]. \tag{52}$$

The Routh-Hurwitz conditions for a stable steady state are $T_1 < 0$, $T_3 < 0$, and $T_1T_2 - T_3 < 0$, which we have verified. Equation (49) admits a pair of complex-conjugate eigenvalues. The imaginary part provides the frequency of the decaying oscillations. In the limit $\eta \to 0$, it is given by

$$\omega = \sqrt{\frac{1}{3}\eta(I_g + 5I_{\rm ex})}. \tag{53}$$

In summary, we found only one RO frequency for the full range of pump currents, and, therefore, no energy exchange between the two modes. The two modes are dynamically identical. The appearance of the ES emission leads only to the dramatic change of slope for the RO frequency versus pump current, as shown in Fig. 4. We also analyzed the case of the GS ($I_g \neq 0$ and $I_{\rm ex} = 0$) and found (53) with $I_{\rm ex} = 0$ as the approximation of the RO frequency. In Fig. 4, we compare the approximation (53) with their values obtained by simulating numerically the linearized equations. Expression (53) reveals a significant difference from the approximations

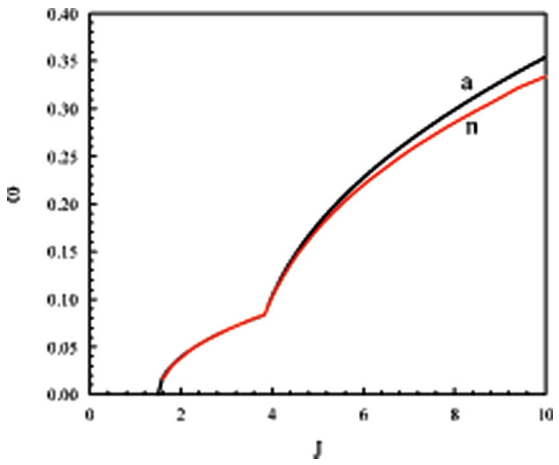

FIG. 4. (Color online) RO frequency. The RO frequency determined numerically (curve n) from Eqs. (7)–(12) is compared to the frequency obtained analytically (curve a) from (53). The fixed parameters are the same as in Fig. 1.

(28) and (29). First, we note that $\omega = \sqrt{\eta I_g/3}$ if $I_{ex} = 0$, which is quantitatively different from (28). Second, the RO frequency (53) is not a direct function of the total intensity $(I_g + I_{ex})$, as we may naively expect. The linear combination of the GS and ES intensities $(I_g + 5I_{ex})$ in (53) is different from the total intensity by a factor 5. Our analysis distinguishes two contributions to the factor, namely, the electron-hole asymmetry, and the higher degeneracy in the ES energy levels. The RO frequency (53) can be reformulated as

$$\omega = \sqrt{\eta\left[\tfrac{1}{6}(2I_g + 4I_{ex}) + \tfrac{1}{4}(4I_{ex})\right]}. \tag{54}$$

The role of the asymmetry relates to the difference between the redistribution rates of the two types of carriers, which results in the faster depopulation of the ES electron level. Therefore, the two types of carriers contribute differently to the laser relaxation process, which results in two terms in (54). The first term $\approx(2I_g + 4I_{ex})$ accounts for the relaxation of the holes. The second term $\approx(4I_{ex})$ relates to the relaxation dynamics of the ES electrons. Both terms explicitly appear in (46). The electron-hole asymmetry provides the most significant contribution to the change of slope for the RO frequency versus pump current.

On the other hand, the higher degeneracy generates a larger ES differential gain, implying a higher contribution to the RO frequency. The difference in the differential gains reveals itself in the factors 2 and 4 in $(2I_g + 4I_{ex})$, which naturally originate from the degeneracy factors.

V. CONCLUSIONS

We analyze intradot interactions in a QD laser operating simultaneously at the GS and ES. The small values of two dimensionless parameters, namely, the normalized photon lifetime $\eta = \tau_{ph}\tau^{-1}$ and the normalized capture time $B^{-1} = \tau_c\tau^{-1}$, allowed us to determine approximations of the RO frequency from a six-variable linear stability problem. If ηB (B fixed) is sufficiently small, the two states are lasing with independent frequencies that are determined by their individual intensities. On the other hand, if ηB small approaches $O(1)$ quantities, a unique frequency appears which depends on a linear combination of the two-state intensities. This combination is not symmetric and reveals the complex nature of the nonlinear intradot interactions. In future work, we plan to consider the case $\eta B = O(1)$ in more detail and evaluate both the RO frequencies and their damping rates.

ACKNOWLEDGMENTS

This work was funded by European Union, Erasmus Mundus External Cooperation Window (EMECW) programme under Project No. 141085-EM-1-2008-BE-ERAMUNDUS-ECW-L02, Belgium. This work has been partially funded by the Research Foundation Flanders (FWO) and the Belgian Science Policy Office under Grant No. IAP-7/35 "photonics@be."

[1] D. Bimberg, M. Grundmann, and N. N. Ledentsov, *Quantum Dot Heterostructures* (Wiley, New York, 1999).
[2] A. Markus, J. X. Chen, C. Paranthoen, A. Fiore, C. Platz, and O. Gauthier-Lafaye, Appl. Phys. Lett. **82**, 1818 (2003).
[3] E. A. Viktorov, P. Mandel, Y. Tanguy, J. Houlihan, and G. Huyet, Appl. Phys. Lett. **87**, 053113 (2005).
[4] M. Gioannini, J. Appl. Phys. **111**, 043108 (2012).
[5] E. A. Viktorov, P. Mandel, I. O'Driscoll, O. Carroll, G. Huyet, J. Houlihan, and Y. Tanguy, Opt. Lett. **31**, 2302 (2006).
[6] E. A. Viktorov, M. A. Cataluna, L. O'Faolain, T. F. Krauss, W. Sibbett, E. U. Rafailov, and P. Mandel, Appl. Phys. Lett. **90**, 121113 (2007).
[7] A. Markus, M. Rossetti, V. Calligari, D. Chek-Al-Kar, J. X. Chen, A. Fiore, and R. Scollo, J. Appl. Phys. **100**, 113104 (2006).
[8] M. A. Cataluna, W. Sibbett, D. A. Livshits, J. Weimert, A. R. Kovsh, and E. U. Rafailov, Appl. Phys. Lett. **89**, 081124 (2006).
[9] M. A. Cataluna, D. Nikitichev, S. Mikroulis, H. Simos, C. Simos, C. Mesaritakis, D. Syvridis, I. Krestnikov, D. Livshits, and E. U. Rafailov, Opt. Exp. **18**, 12832 (2010).
[10] T. Erneux and P. Glorieux, *Laser Dynamics* (University Press, Cambridge, UK, 2010).
[11] P. Mandel, *Theoretical Problems in Cavity Nonlinear Optics* (Cambridge University Press, Cambridge, UK, 2005).
[12] T. Erneux, E. A. Viktorov, and P. Mandel, Phys. Rev. A **76**, 023819 (2007).
[13] K. Lüdge, E. Schoell, E. A. Viktorov, and T. Erneux, J. Appl. Phys. **109**, 103112 (2011).
[14] P. Moreno, F. Salleras-Vila, A. Markus, A. Crottini, M. A. Dupertuis, J. X. Chen, B. Deveaud, and A. Fiore, in *Proceedings of the European Quantum Electronics Conference*, Munich (IEEE, New York, 2005).
[15] L. V. Asryan and R. A. Suris, Semicond. Sci. Technol. **11**, 554 (1996).
[16] K. Veselinov, F. Grillot, Ch. Cornet, J. Even, A. Bekiarski, M. Gioannini, and S. Loualiche, IEEE J. Quantum Electron. **43**, 810 (2007).
[17] P. Mandel, K. Otsuka, J. Y. Wang, and D. Pieroux, Phys. Rev. Lett. **76**, 2694 (1996).
[18] T. Erneux and P. Mandel, Phys. Rev. A **52**, 4137 (1995).